Journal of Molecular Catalysis A: Chemical 339 (2011) 52–60

Contents lists available at ScienceDirect

Journal of Molecular Catalysis A: Chemical

journal homepage: www.elsevier.com/locate/molcata

The effect of rare earth modification on ceria–zirconia solid solution and its application in Pd-only three-way catalyst

Qiuyan Wang[a], Guangfeng Li[a], Bo Zhao[a,b], Renxian Zhou[a,*]

[a] Institute of Catalysis, Zhejiang University, Hangzhou 310028, PR China
[b] School of Pharmaceutical and Chemical Engineering, Taizhou University, Taizhou 317000, PR China

ARTICLE INFO

Article history:
Received 1 November 2010
Received in revised form 15 February 2011
Accepted 17 February 2011
Available online 26 February 2011

Keywords:
$Ce_{0.2}Zr_{0.8}O_2$
Rare earth
Structural modification
Pd-only three-way catalyst

ABSTRACT

The influence of rare earth elements (La, Nd, Pr, Sm and Y) addition to $Ce_{0.2}Zr_{0.8}O_2$ and its supported Pd-only three-way catalysts has been investigated by X-ray diffraction (XRD), N_2 adsorption/desorption, X-ray photoelectron spectroscopy (XPS) and H_2 temperature programmed reduction (H_2-TPR) techniques, and that the dynamic oxygen storage capacity (DOSC) has also been evaluated under transient conditions. Special attention was given to the information of structural modification and the effect of doping on the three-way catalytic performance. The phase for all the ceria–zirconia-rare earth ternary solid solution is single tetragonal, irrespective of the treatment temperature applied. The presence of La, Nd and Pr results in enhanced thermal stability, improved reducibility and increased strong metal–support interaction, leading to the relatively higher three-way catalytic activity for all the target pollutants over the corresponding catalysts. The air/fuel operation window is also enlarged due to the increased dynamic oxygen storage capacity.

1. Introduction

Recently, air pollution mainly generated from gasoline engine powered vehicles has attracted growing attention [1–3]. Emission regulations introduced in every country since the second half of 1990s are more severe than earlier standards. As a result of these tightened legislations and the demands for environmental protection, development of new type three-way catalysts (TWC) is required, which are able to remove all three pollutants CO, NO_x and HC (hydrocarbons) in gasoline engine exhausts simultaneously.

Oxygen storage materials (OSM), typically cerium oxide, are one of the key components in TWC. Its major role is to stores oxygen under oxygen excess conditions and releases it under oxygen deficient conditions on the basis of the reversible redox reaction between Ce^{3+} and Ce^{4+}, i.e., oxygen storage capacity (OSC). It means that OSM provides a way to minimize the fluctuation of air/fuel (A/F) ratio at 14.6 during the engine operation, thus ensuring that TWC works efficiently within a narrow operating window near the stoichiometric [4–6]. Moreover, OSM also can promote the noble metal dispersion, increase the thermal stability of TWC, accelerate the water–gas shift and steam reforming reactions, and favor catalytic activity at the interface of metal–support [7,8]. However, cerium oxide readily sinters upon thermal treatment, leading to the loss of oxygen storage capacity and further the deactivation of catalytic activity. The advent of ceria–zirconia mixed oxide and especially the formation of ceria–zirconia solid solution as the new generation of oxygen storage component usher in a step change in the catalytic performance [9]. On the one hand, the insertion of ZrO_2 into the CeO_2 results in increased thermal stability [10] and promoted reducibility of the mixed oxides [11]. On the other hand, distortion of O^{2-} sublattice in the mixed oxides permits a higher mobility of the lattice oxygen, giving rise to the enhanced OSC [12,13]. It is well known that OSC is currently used as one of the key parameters for evaluating the practicability of oxygen storage materials in TWC, and it is usually measured using the pulse injection method initially developed by Yao and Yu Yao [14]. H_2 molecular species was used to measure the oxygen in the samples, and the amount of O_2 consumed during the re-oxidation stage of the pulse experiment was referred as the oxygen storage capacity complete (OSCC). The amount of CO consumed, measured during a step alternating gas concentration switch 4% CO/1% Ar/He → He → 2% O_2/1% Ar/He, was defined as dynamic oxygen storage (DOSC) [15,16]. Instead of the static or theoretical oxygen storage capacity, the dynamic oxygen storage capacity relates more closely with the practical catalytic process.

In practice, TWC is located in positions closer to the engine manifold in order to reduce emissions during the cold-start period. This results in extreme catalyst temperature which may exceed 1000 °C [17,18]. Therefore, the thermal stability of ceria–zirconia mixed oxides is still highly desired to enhance. A considerable number of studies have been directed toward understanding the intrinsic properties of ceria–zirconia solid solution [19–24],

* Corresponding author. Tel.: +86 571 88273290; fax: +86 571 88273283.
E-mail address: zhourenxian@zju.edu.cn (R. Zhou).

1381-1169/$ – see front matter.
doi:10.1016/j.molcata.2011.02.011

and it has been proved that the properties are affected by the composition strongly. Therefore, we have studied the properties of ceria–zirconia solid solution with different composition and it was found that $Ce_{0.2}Zr_{0.8}O_2$ shows the preferable thermal stability, indicating the practicality of Zr-rich ceria–zirconia solid solution, to which only a small amount of researchers pay attention. However, the low content of ceria results in unsatisfied OSC, which restricts the development of Zr-rich solid solution.

As literature reported [1,25–32], the addition of rare earth is beneficial to enhance the properties of ceria–zirconia solid solution. In our previous work [33], we have initiated a preliminary research on the rare earth (La, Nd, Pr, Sm and Y) modified $Ce_{0.2}Zr_{0.8}O_2$, and the effect of rare earth doping was mainly investigated from a structural and textural point of view. However, to better understand the effect of rare earth modification on the Zr-rich ceria–zirconia solid solution and the corresponding Pd-only three-way catalyst, more intensive work is needed. The current research interest is thus focused on the in-depth study using X-ray photoelectron spectroscopy (XPS) technique and dynamic oxygen storage capacity (DOSC) investigation chiefly.

2. Experimental

2.1. Catalyst preparation

The rare earth element doped CZ (CZRe) was prepared by coprecipitation method and the pure CZ was also prepared as a reference. The ammonia solution was slowly added to the quantitative mixed aqueous solution of corresponding nitrates under continuous stirring until pH 9.0. The resulting precipitate was filtered, extensively washed with distilled water, and then washed with ethanol furthermore to replace the water in the precipitate considering that it would be dried by supercritical method in ethanol atmosphere subsequently (265 °C, 7.0 MPa). The molar ratio of Ce/Zr is 1:4, and the content of relevant rare earth is 5 wt.% for CZRe. After calcination at 500 °C for 4 h, the materials were crushed followed by sieved to a size range of 40–60 mesh, and then the so-called fresh supports were obtained. For the sake of convenience, the fresh supports modified by La, Nd, Pr, Sm and Y were denoted as CZL, CZN, CZP, CZS and CZY, respectively. All the samples were calcined at 1100 °C for 4 h to investigate the effect of rare earth doping on the thermal stability of ceria–zirconia solid solution, and the aged samples were referred to as CZa, CZLa, CZNa, CZPa, CZSa and CZYa, correspondingly.

The Pd/CZ and Pd/CZRe catalysts were prepared by conventional impregnation with an aqueous of H_2PdCl_4 as metal precursor. The impregnated samples were reduced with hydrazine hydrate to deassociate Pd^{2+} and Cl^- via the transformation of Pd^{2+} to Pd. Then the reduced sample was filtered and washed with a large amount of deionized water until no Cl^- ion was detected in the filtered solution (by $AgNO_3$ aqueous), considering that the appearance of Cl is harmful to the catalytic activity. The washed samples were dried at 110 °C for 4 h and then calcined at 500 °C for 2 h due to the active phase in TWC is metal oxide. In order to compare their thermal stability, the catalysts were also calcined at 1100 °C for 4 h. The theoretical loading content of Pd for all catalysts is 0.5 wt.%. The catalysts obtained at 1100 °C were labeled as Pd/CZa and Pd/CZRea, respectively.

2.2. Catalytic activity test

The evaluation of three-way catalytic activity was performed in a fixed-bed quartz reactor. The catalyst (0.2 ml, 40–60 m) was held in the quartz tube by packing quartz wool at both ends of the catalysts bed, and the back-mixing in reactor is minimized by decreasing the dead volume of the reactor. The feed stream was regulated using special mass flow controllers and contained NO (0.1%)–NO_2 (0.03%)–C_3H_6 (0.067%)–C_3H_8 (0.033%)–CO (0.75%)–O_2 (0.745%) with balance Ar and the space velocity was 43,000 h^{-1} referred to the catalyst volume and to a gas flow rate at room temperature (25 °C). The contents of CO, NO, NO_2 and total HC (C_3H_6 and C_3H_8) were recorded by a Bruker EQ55 FTIR spectrometer coupled with a multiple reflection transmission cell (Infrared Analysis Inc.) before and after the simulated gas passed the reactor. The existence of small quantity of H_2O has been confirmed by mass spectrum (QIC-20 gas analytical system, England) in the feed gas stream. It means that H_2O also participated in the three-way catalytic reaction in our study. However, the evaluation of three-way catalytic activity was performed by a Bruker EQ55 FTIR spectrometer, and the detection of H_2O would inflict serious damage to this instrument. Therefore, the concentration of H_2O was not given. Moreover, H_2O produced in the process of reaction was also removed before the tail gas passed through the multiple reflection transmission cell.

The air/fuel ratio experiments were carried out at 400 °C. The λ value of the simulated exhaust, which represents the ratio between the available oxygen and the oxygen needed for full conversion to CO_2, H_2O, and N_2, is defined as $\lambda = (2V_{O_2} + V_{NO} + 2V_{NO_2})/(V_{CO} + 9V_{C_3H_6} + 10V_{C_3H_8})$ [34–36] (V means concentration in volume percent unit). λ = 1 was utilized in all the activity measurements, while the test of air/fuel operation window was carried out at λ = 0.9, 0.92, 0.95, 0.98, 1.0, 1.04, 1.07, 1.1 and 1.15, respectively.

2.3. Characterization techniques

Powder X-ray diffraction (XRD) patterns were recorded by an ARL X'TRA diffractometer using nickel-filtered Cu Kα radiation operating at 40 kV and 40 mA and with 0.02° step size scanning from 20° to 80° (2θ).

BET surface areas of the samples were determined by nitrogen physisorption at 77 K using a Coulter OMNISORP-100 apparatus, after degassing the samples in vacuum (<10^{-5} Torr) at 200 °C for 2 h.

The X-ray photoelectron spectroscopy (XPS) experiments were carried out on a PHI-Quantera SXM system equipped with a monochromatic Al Kα X-rays under ultra-high vacuum (6.7×10^{-8} Pa). Sample charging during the measurement was compensated by an electron flood gun. The XPS data from the regions related to C 1s, O 1s, Zr 3d, Ce 3d, Re 3d and Pd 3d core levels were recorded for each sample. The binding energies were calibrated internally by the carbon deposit C 1s binding energy (BE) at 284.8 eV. The deconvolution method of XPS spectra is fitted by Gaussian function.

The dynamic oxygen storage capacity (DOSC) measurements with CO–O_2 pulse were operated at 400 °C. CO (4% CO/1% Ar/He at 300 ml/min for 10 s) and O_2 (2% O_2/1% Ar/He at 300 ml/min for 10 s) streams were pulsed alternatively with a pulsation frequency (i.e., the number of times CO–O_2 pulse was performed per second) of 0.05 Hz. Prior to the DOSC measurement, all the catalysts were first pretreated in O_2 at 400 °C for 10 min followed by He purge for 5 min. A DOSC value was obtained by integrating the CO_2 formed during one CO-O_2 cycle and was expressed as μmol of O per gram of catalyst (μmol [O]/g).

Temperature programmed reduction (TPR) measurements were carried out on a GC-1690 chromatography to observe the reducibility of samples. Prior to H_2-TPR measurement, 50 mg sample was pretreated at 300 °C in air for 0.5 h. The reducing gas was a mixture of 5 vol.% H_2 in Ar (40 ml/min), which was purified using deoxidizer and silica gel. The experimental temperature was raised at a constant rate of 10 °C/min. The consumption of hydrogen during the reduction was measured by a thermal conductivity detector

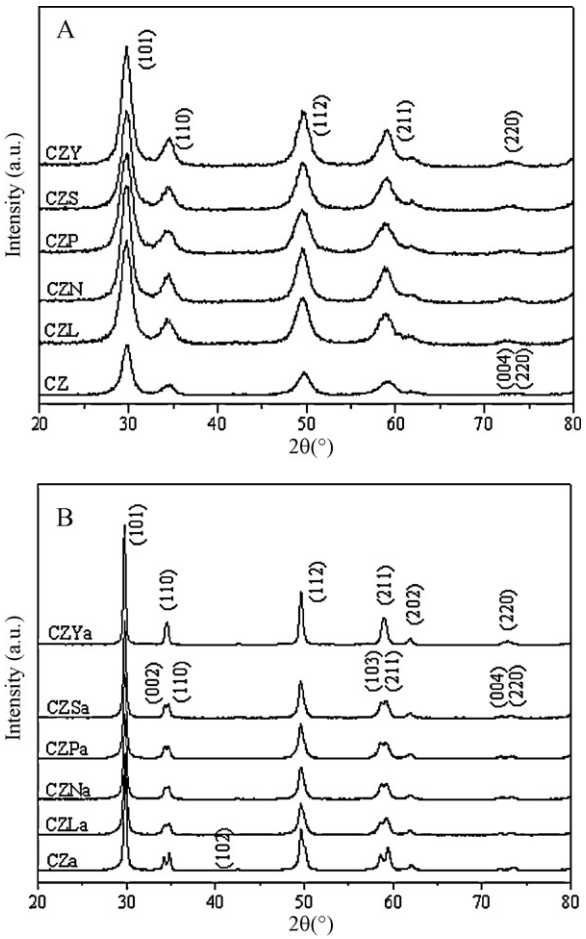

Fig. 1. XRD patterns of supports calcined at 500 °C (A) and 1100 °C (B).

(TCD), and the water formed during H_2-TPR was absorbed with 5A molecular sieve.

3. Results and discussion

3.1. Structural and textural properties

The results of structural and textural characterization for all the fresh and aged supports were summarized in Tables 1 and 2, respectively. The XRD patterns for all the samples were displayed in Fig. 1. According to cerium content, the ceria–zirconia solid solutions exist in three different structures, namely monoclinic, tetragonal and cubic [17]. As shown in Fig. 1A, for all the fresh supports, the XRD patterns feature broad and symmetric peaks with low intensity, indicating the formation of nanostructure [34], as evidenced by the small crystallite size shown in Table 1. The main peaks between 20° and 80° are related to tetragonal ceria–zirconia solid solution (space group $P_{42}/nmcs$, $Z = 2$, ICSD No. 68590) due to Zr-rich in the component. Moreover, no diffraction peaks of rare earth are observed. From Table 1, it can be seen that the lattice parameters for all the rare earth doped samples are larger than that of pure CZ, indicating the insertion of rare earth ion into the lattice of ceria–zirconia solid solution. Based on the statement presented above, the formation of ceria–zirconia-rare earth ternary solid solution could be confirmed.

For all the rare earth elements shown in this work, the ionic radius of Re^{3+} is smaller than that of Ce^{3+} (1.14 Å). Therefore, the substitution of Ce^{3+} by Re^{3+} is unbelievable for it would lead to the lattice shrinkage. For CZL, CZN and CZP, the radius of La^{3+} (1.06 Å), Nd^{3+} (1.00 Å) and Pr^{3+} (1.01 Å) are larger than that of both Ce^{4+} (0.97 Å) and Zr^{4+} (0.84 Å). However, the ionic radius of Ce^{4+} is close to La^{3+}, Nd^{3+} and Pr^{3+}. Although Ce^{4+} could be substituted by them, the amount must be very little for it cannot account for the obviously lattice expansion. On the other hand, the content of Ce in the ceria–zirconia is relatively little (the theoretical molar ratio of Ce to Zr is 1:4). Therefore, the cation site substitution of Zr by La, Nd and Pr in corresponding CZL, CZN and CZP seems more credible. With regard to CZS and CZY, the ionic radius of Sm^{3+} and Y^{3+} is 0.96 Å and 0.89 Å, which is only larger than that of Zr^{4+}. Hereby, the substitution of Zr by Sm and Y in CZS and CZY is reasonable. Altogether, it can be point out that the formation of ceria–zirconia-rare earth ternary solid solution is facile and Zr is replaced by Re mainly in the framework of ternary solid solution.

The values of specific surface area, mean pore size and cumulative pore volume of the fresh supports detected by N_2 adsorption/desorption were also given in Table 1. As displayed in Table 1, the addition of rare earth into the ceria–zirconia solid solution results in the increased BET surface area and pore volume, proving the enhanced textural stability. The analysis of t-plots reveals that the fresh supports have a higher incidence of mesopore with wide pore size distribution. In literature [35], we have proved that this special structure results from the adoption of supercritical drying method is beneficial to the adsorption/desorption of pollutants in TWC.

After treatment at 1100 °C for 4 h (Fig. 1B), the reflections of the aged supports become sharper and more intense when comparing with the fresh one. The separation of peaks around 35°, 58° and 72° as well as a weak peak around 42.5° are observed. All the additional characteristic peaks are also consistent with the tetragonal structure. These observations indicate the formation of larger crystallite caused by the serious sintering, which agrees well with the increased crystalline size as depicted in Table 2. However, the degree of peak splitting and the grain size for the rare earth modified supports is smaller than CZa, indicating that the sintering of the aged supports is clearly attenuated due to the introduction of rare earth. A clearly defined decrease in BET surface area and pore volume as well as the increase in mean pore diameter is obtained when comparing the aged supports with the fresh ones, which is caused by the agglomeration occurred during the high temperature treatment. However, the aged samples doped with La, Nd and Pr also show higher specific surface area than CZa.

3.2. XPS

XPS investigation was conducted to provide information of the surface elemental distribution. The alteration of chemical state of cerium upon partial fresh and aged catalysts was shown in Fig. 2 representatively. The surface elemental contents calculated from the normalized peak areas of the Ce 3d, Zr 3d, Re 3d, Pd 3d and O 1s core level spectra and the relative concentration of Ce^{3+} for the fresh and aged catalysts were listed in Tables 3 and 4, respectively.

The curve of Ce 3d spectra shown in Fig. 2 comprises eight peaks corresponding to four pairs of spin–orbit doublets. Early studies [37–39] have shown that Ce $3d_{3/2}$ multiplets are labeled as u, whereas those of $3d_{5/2}$ are labeled as v. Specifically, the peaks marked as u, u″ and u‴ arise from Ce^{4+} $3d_{3/2}$ while the peaks denoted as v, v″ and v‴ arise from Ce^{4+} $3d_{5/2}$, the couples corresponding to one of the two possible electron configuration of the final state of the Ce^{3+} species are labeled as u′ and v′. The relative percentages of cerium species are obtained by the area ratios of Ce^{4+} $3d_{5/2}$ (v, v″ and v‴)/Ce^{3+} $3d_{5/2}$ (v′). From Table 3, it can be known that all the rare earth doped samples show higher relative concentration of Ce^{3+} than Pd/CZ. Summarizing the literature [37,40], it is generally recognized that the presence of Ce^{3+} is associated with

Table 1
BET surface area, lattice constants, crystallite size, pore volume and mean pore diameter for fresh supports.

Samples	Surface area (m^2/g)	Lattice constants (Å)	Crystallite size (Å)	Pore volume (cm^3/g)	Mean pore diameter (nm)
CZ	105.9	$a=b=3.625$, $c=5.218$	6.7	0.407	17.41
CZL	144.4	$a=b=3.661$, $c=5.228$	5.8	0.628	18.22
CZN	127.1	$a=b=3.655$, $c=5.217$	6.5	0.551	17.57
CZP	157.8	$a=b=3.658$, $c=5.224$	5.1	0.668	17.21
CZS	127.5	$a=b=3.651$, $c=5.215$	6.0	0.545	16.51
CZY	127.5	$a=b=3.648$, $c=5.215$	6.5	0.567	17.56

Table 2
BET surface area, lattice constants, crystallite size, pore volume and mean pore diameter for aged supports.

Samples	Surface area (m^2/g)	Lattice constants (Å)	Crystallite size (Å)	Pore volume (cm^3/g)	Mean pore diameter (nm)
CZa	24.3	$a=b=3.632$, $c=5.227$	32.2	0.034	22.56
CZLa	39.6	$a=b=3.644$, $c=5.232$	20.4	0.126	22.03
CZNa	28.8	$a=b=3.648$, $c=5.224$	19.5	0.087	20.15
CZPa	27.6	$a=b=3.644$, $c=5.225$	17.2	0.061	22.05
CZSa	21.0	$a=b=3.647$, $c=5.220$	29.1	0.042	21.27
CZYa	19.4	$a=b=3.654$, $c=5.200$	16.9	0.032	18.60

Table 3
Surface composition and surface atom ratio of the fresh catalysts derived from XPS analyses.

Sample	Surface composition (at.%)					Zr/Ce	Ce^{3+} $3d_{5/2}$ in Ce (%)
	Ce 3d	Zr 3d	Re 3d	Pd 3d	O 1s		
Pd/CZ	2.88	13.68	0	–	83.44	4.75	17.29
Pd/CZL	2.75	12.51	0.55	–	84.19	4.55	23.41
Pd/CZN	2.84	13.41	0.09	–	83.66	4.72	19.64
Pd/CZP	2.66	12.39	0.81	–	84.14	4.66	18.98
Pd/CZS	2.82	13.32	0.52	–	83.34	4.72	18.13
Pd/CZY	2.83	13.32	0.29	–	83.56	4.71	18.37

the formation of oxygen vacancies according to the electroneutrality condition. Therefore, we can conclude that the introduction of rare earth into CZ solid solution increases the oxygen vacancies on the surface of sample.

As shown in Table 3, no Pd is observed in the case of all the fresh catalysts. There are two possible reasons. One is the loading content of Pd is extremely low, which approaches the limit detection (0.5 wt.%). The other is the Pd appeared on the surface of the catalysts may be highly dispersed. In addition, the surface atom ratios of Zr/Ce over Pd/CZRe are smaller than that over Pd/CZ, which means that part of Zr atoms in the surface layer is replaced by Re. After aging at 1100 °C for 4 h, the surface content of Re increases significantly as a result of the migration of Re from bulk to surface [41]. Table 4 shows that Pd is detectable in the case of aged catalysts, indicating the obvious sintering of noble metal due to the high temperature treatment. However, the content of Pd on the surface of Pd/CZLa, Pd/CZNa and Pd/CZPa is lower than that on the surface of Pd/CZa. On the contrary, the content of Pd on the surface of Pd/CZSa and Pd/CZYa is higher than that on the surface of Pd/CZa. This observation implies that the addition of La, Nd and Pr would improve the

Table 4
Surface composition and surface atom ratio of the aged catalysts derived from XPS analyses.

Sample	Surface composition (at.%)					Zr/Ce	Ce^{3+} $3d_{5/2}$ in Ce (%)
	Ce 3d	Zr 3d	Re 3d	Pd 3d	O 1s		
Pd/CZa	3.42	12.23	0	0.04	84.31	3.58	15.21
Pd/CZLa	3.16	11.88	1.33	0.02	83.61	3.76	21.65
Pd/CZNa	3.75	11.69	0.18	0.02	84.36	3.12	17.04
Pd/CZPa	3.31	11.44	1.20	0.03	84.02	3.46	16.87
Pd/CZSa	3.14	12.77	0.61	0.07	83.41	4.07	16.54
Pd/CZYa	2.67	11.71	1.04	0.07	84.51	4.37	15.52

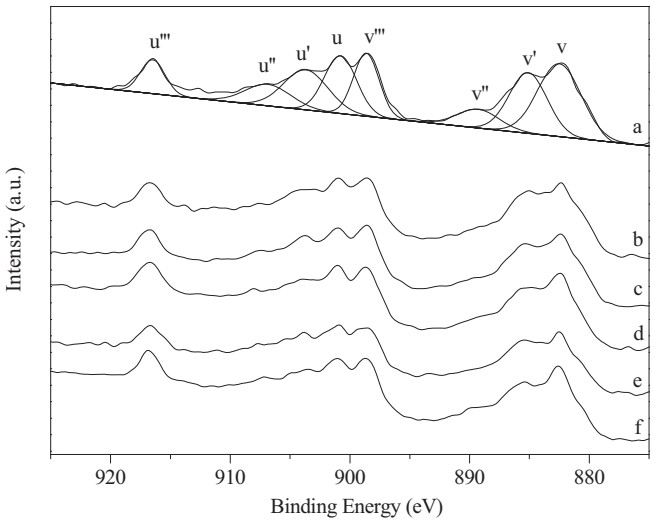

Fig. 2. Ce 3d XP-spectra of representative catalysts: (a) Pd/CZ, (b) Pd/CZL, (c) Pd/CZS, (d) Pd/CZa, (e) Pd/CZLa and (f) Pd/CZSa.

strong metal–support interaction (SMSI), inhibiting the sintering of noble metal on the interface of support. What should be mentioned is that the relative concentration of Ce^{3+} on the surface of rare earth doped samples is also higher than that on the surface of Pd/CZa, especially for Pd/CZLa.

3.3. DOSC

The representative evolution curves of CO, O_2 and CO_2 during the process of alternative dynamic pulse of 4% CO/1% Ar/He and 2% O_2/1% Ar/He under 0.05 Hz over Pd/CZ was shown in Fig. 3, where only three CO–O_2 cycle is selected from the continuous transient CO–O_2 pulses to represent the dynamic OSC curve. Fig. 4 displayed the CO_2 evolution curves during alternating CO and O_2 pulses at 400 °C over Pd/CZ, Pd/CZL, Pd/CZS and the corresponding aged catalysts, representatively. The corresponding DOSC amounts are calculated by integrating the peak area under the CO_2 curve during one CO–O_2 cycle.

The behavior of bimodal CO_2 curves under single CO–O_2 cycle shown in Fig. 4 is in good agreement with the results described in other research [6,42–45]. The CO_2 peak appears at the start of the

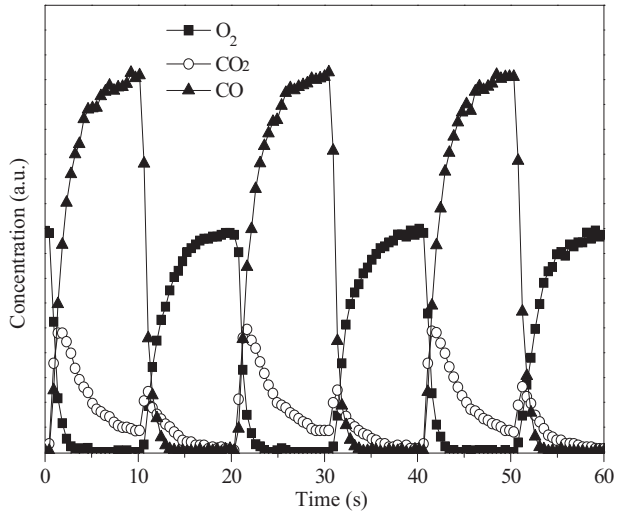

Fig. 3. Representative transition curve with alternate dynamic pulses of 4% CO/1% Ar/He (10 s) and 2% O_2/1% Ar/He (10 s) under 0.05 Hz over Pd/CZ.

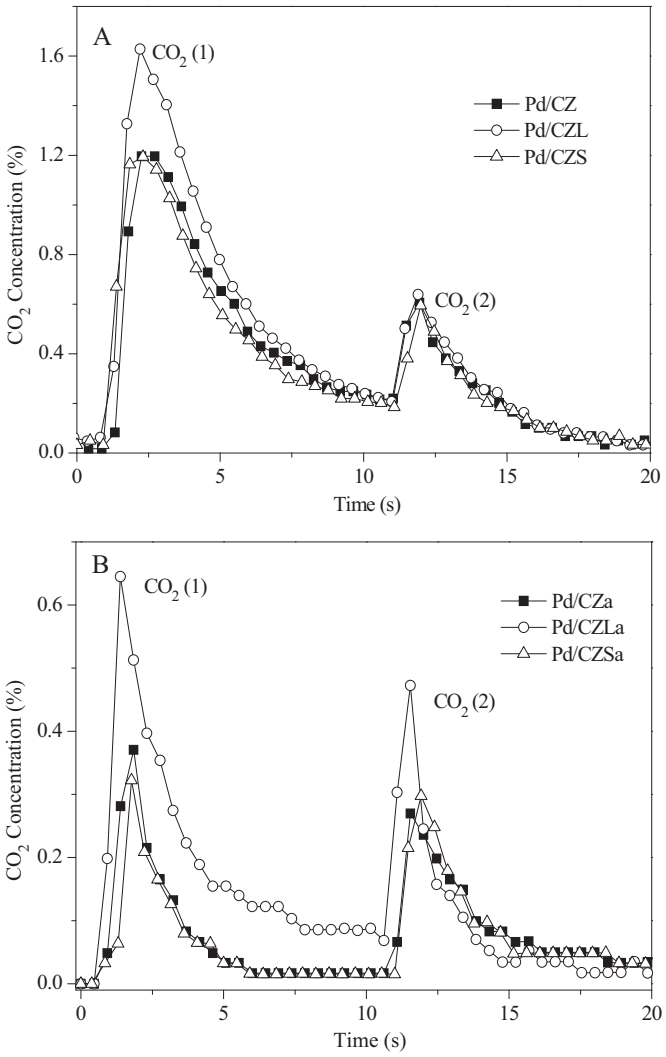

Fig. 4. The representative CO_2 response peaks with alternate dynamic pulses of 4% CO/1% Ar/He and 2% O_2/1% Ar/He under 0.05 Hz over fresh (A) and aged (B) catalysts.

CO pulse is designated as CO_2 (1) and the second peak is labeled as CO_2 (2). According to Descorme et al. [43] and Boaro et al. [44], the coexistence of CO and gaseous O_2 should be taken into the analysis of CO_2 concentration curves. In the case of CO_2 (1), since the catalyst is partially oxidized before the introduction of CO, the CO_2 formation included CO_2 generating from both the catalytic oxidation of CO in the presence of gaseous oxygen and the oxygen release reaction. Christou et al. [46] have developed a two-step Eley–Rideal (E–R) reaction mechanism that involves the reaction of gaseous CO with the oxygen species of PdO and of the back-spillover of oxygen form oxygen storage material to the oxygen vacant sites of surface PdO. The formation of CO_2 (2) is completely attributed to the catalytic oxidation of CO since the oxides are partially reduced at this moment. Fan et al. [39] confirmed the existence of catalytic oxidation of CO by gaseous O_2 via comparing the CO step in CO–O_2 cycles and the first pulse in the successive CO pulse measurement. Meanwhile, the effect of carbonate formation is proposed after in situ DRIFTS inspection of the reactions during the CO–O_2 cycles. To sump up, CO oxidation by mixed oxides and gaseous oxygen, carbonate formation and decomposition are all responsible for the bimodal profiles of CO_2 in DOSC test.

The DOSC values of all the fresh and aged catalysts were presented in Fig. 5. From Fig. 5, it can be seen that the DOSC values of the fresh catalysts follow the sequence of

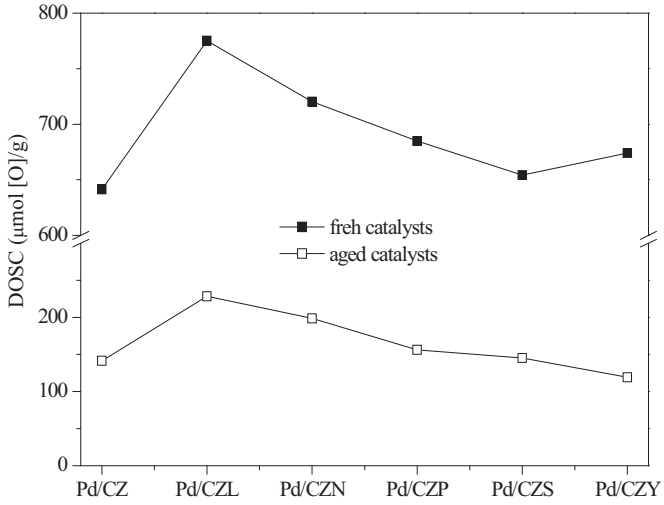

Fig. 5. The DOSC values of all the fresh and aged catalysts.

Pd/CZL > Pd/CZN > Pd/CZP > Pd/CZY > Pd/CZS > Pd/CZ, which is in consistent with the decreasing sequence of relative concentration of Ce^{3+} on the surface of fresh catalysts (as shown in Table 3). After calcination at 1100 °C for 4 h, the DOSC value of aged catalyst is decreased obviously compared with the corresponding fresh one. The E–R mechanism [46,47], which has been developed and widely accepted to explain the inherent of DOSC behavior, is based on the following two mechanistic steps:

$$CO(g) + O\text{-}s_1 \rightarrow CO_2(g) + s_1 (k_1, \text{step1})$$

$$O\text{-}s_2 + s_1 \rightarrow O\text{-}s_1 + s_2 \ (k_2^{app}, \ \text{step 2})$$

where s_1 denotes an oxygen vacant adsorption site on the PdO surface, s_2 denotes a site on support where an adsorbed oxygen and/or lattice oxygen species is associated with, k_1 is the intrinsic rate constant of elementary step 1 (CO oxidation reaction), and k_2^{app} is an apparent rate constant associated with the kinetics of the back-spillover of oxygen process from support to the surface of PdO. Both the PdO agglomeration and the deterioration of the structure of support occur after the high temperature treatment. Therefore, the oxygen vacant adsorption site on the PdO surface and on the support would decline obviously, that is why the DOSC of the aged catalyst is lower than the corresponding fresh one. What should be mentioned is that the aged catalysts modified with rare earth exhibit higher DOSC than Pd/CZa, which can also be attributed to the higher Ce^{3+} concentration on the surface of aged catalysts.

3.4. H_2-TPR

The reducibility of supported TWC is an important factor influencing its catalytic performance and H_2-TPR is a common technique to investigate the reducibility of samples [48–50]. The results of consecutive TPR profiles of the fresh and aged supports were presented in Fig. 6, and the H_2-TPR profiles obtained over the fresh and aged catalysts were displayed in Fig. 7.

From Fig. 6A it can be seen that all the fresh supports feature one dominant broad peak with maximum at ca. 550 °C. The previous literatures [17,51] have reported that two peaks at about 500 and 800 °C are found in the TPR profile of ceria–zirconia mixed oxide, which are associated with the reduction at the surface and in the bulk. Therefore, all the peaks appear in the case of fresh supports is more likely to be related to the reduction of surface oxygen. Moreover, all the rare earth doped samples show lower peak temperature than CZ, proving the enhanced reducibility of CZ due to the formation of ternary solid solution. After treatment at 1100 °C for 4 h, the H_2-TPR behavior of the aged supports changes obviously in comparison with the fresh ones. As illustrated in Fig. 6B, two main reduction peaks are observed for CZa, CZLa and CZNa. The peak located at relatively lower temperature is denoted as peak α and the other one is labeled as peak β, which are ascribed to the reduction of surface and sub-surface oxygen [6,52,53], respectively. The splitting of surface oxygen into separated surface and sub-surface oxygen indicates that the declined homogeneity of the fresh supports due to the high temperature calcination. For CZPa, CZSa and CZYa, a broad reduction peak is observed, which may be related to the reduction of bulk oxygen considering that the peak temperature is relatively high.

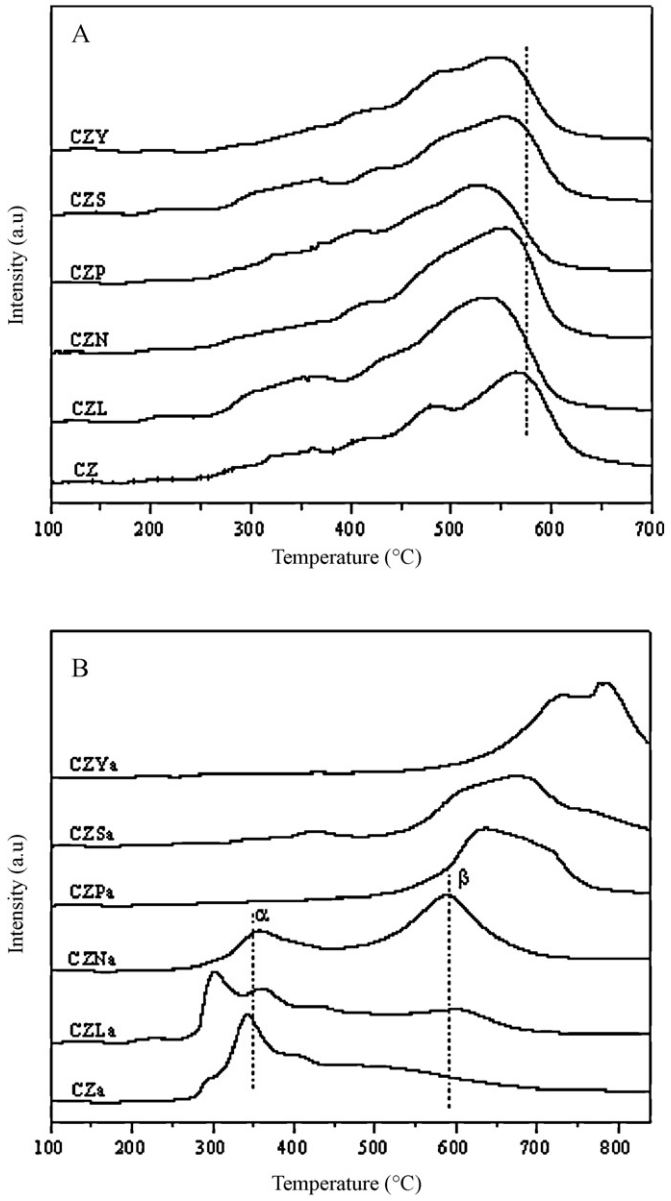

Fig. 6. H_2-TPR traces for the fresh (A) and aged (B) supports.

As shown in Fig. 7A, all of the fresh catalysts exhibit a strong low-temperature reduction feature at ca. 65 °C (peak α) and three tiny peaks in the range of 150–400 °C, namely peak β, γ and δ. Peak α is attributed to the reduction of PdO species, while peak β, γ and δ is associated with the reduction of surface oxygen [35,41]. Based on the amount of H_2 consumption observed over a standard CuO sam-

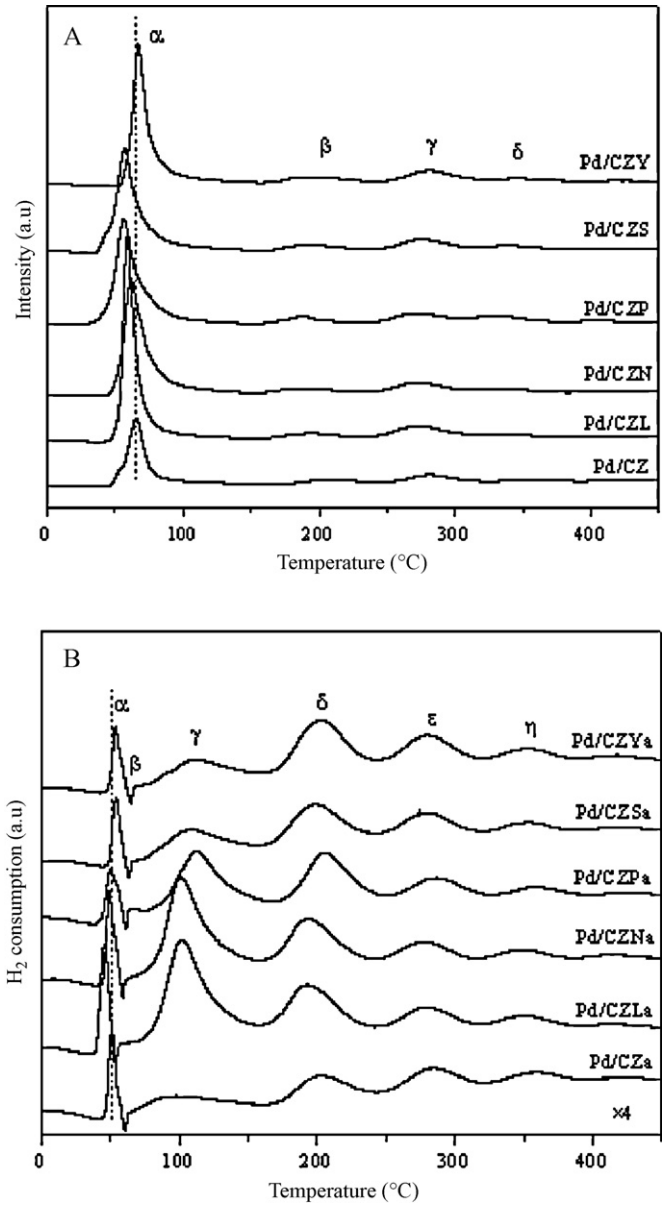

Fig. 7. H_2-TPR traces for the fresh (A) and aged (B) catalysts.

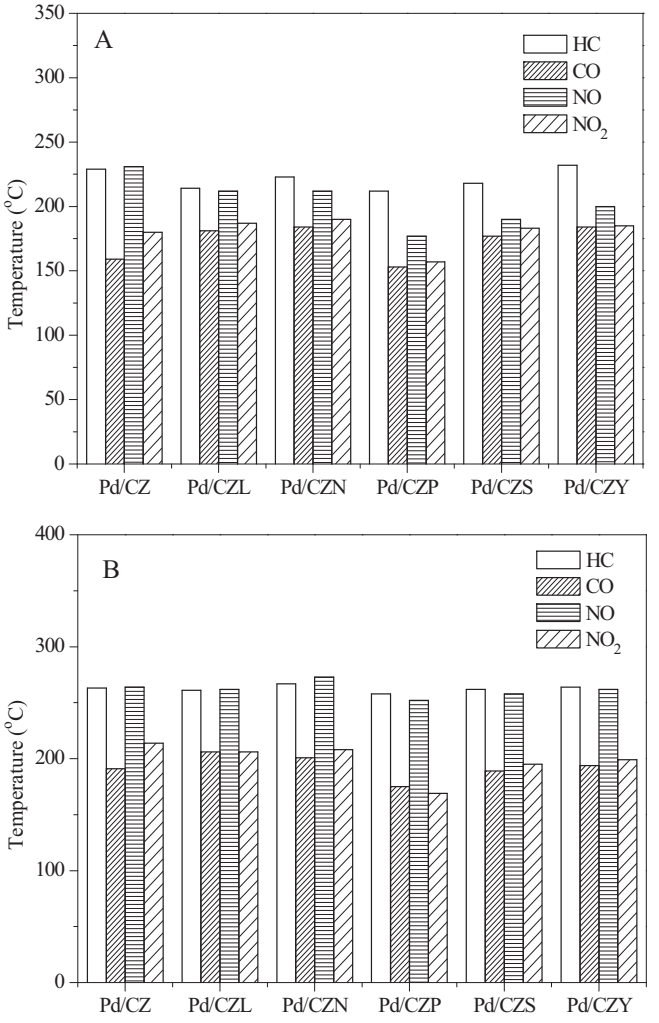

Fig. 8. The light-off temperature (A) and full-conversion temperature (B) over the fresh catalysts.

ple in similar TPR procedures, it is noticed that the total amount of the H_2 consumption for peak α is too large to be reasonably attributed to the reduction of noble metal oxides absolutely, indicating the back-spillover of the oxygen process from the support to the PdO surface [46,47]. For instance, the H_2 consumption for theoretical PdO is just 41 μmol/gcat, while that for peak α in the case of Pd/CZ is 423 μmol/gcat. Therefore, we can conclude that there is a strong interaction between PdO and the support.

With regard to the aged catalysts (as shown in Fig. 7B), the intensity of peak α decreases obviously after calcination at 1100 °C. Papavasiliou et al. [34] have reported that the fresh three-way catalysts prepared by wet impregnation method show high noble metal dispersion values, and a strong reduction of dispersion takes place after thermal aging. Therefore, the decrease of peak α intensity could be attributed to the agglomeration of PdO particles, that is to say, the decrease of PdO dispersion. The negative peak at ca. 60 °C (peak β) is generally attributed to the decomposition of palladium hydride formed following PdO reduction. Peak γ is suggested to the reduction of stable PdO formed on the interaction between PdO and the support [54,55]. A careful comparison of TPR profiles in Fig. 7A shows that the intensity of peak γ for Pd/CZLa, Pd/CZNa and Pd/CZPa is stronger than the others, indicating that the addition of La, Nd and Pr could stabilize the PdO active species due to the SMSI mentioned above. Contrarily, the intensity of peak γ is relatively lower in the case of Pd/CZa, Pd/CZSa and Pd/CZYa. Similarly to the fresh catalysts, peak δ, ε and η are also suggested to the reduction of surface oxygen from the support.

3.5. Catalytic performance

The results of light-off temperature ($T_{50\%}$) and full-conversion temperature ($T_{90\%}$) for CO, HC, NO and NO_2 over the fresh catalysts were given in Fig. 8, while the results of corresponding aged catalysts were summarized in Table 5. From Fig. 8, it appears that the differences of catalytic activity among the fresh catalysts are very slight. Combined with the results of literature [34] and the fact that no distinct Pd is detected in the analysis of XPS, we can conclude that the similar catalytic behavior for the fresh catalyst may be attributed to the indistinguishable high PdO dispersion. For the aged catalysts, a large drop of catalytic activity can be seen from the increase of $T_{50\%}$ and $T_{90\%}$ compared with the fresh catalysts, attributing to the deteriorated structure and the sintering of active component. In the light off test of the aged catalysts, Pd/CZLa, Pd/CZNa and Pd/CZPa are active in pro-

Table 5
Light-off ($T_{50\%}$) and full-conversion ($T_{90\%}$) temperature of HC, CO, NO, and NO_2 over the aged catalysts.

Catalyst	$T_{50\%}$ (°C)				$T_{90\%}$ (°C)			
	HC	CO	NO	NO_2	HC	CO	NO	NO_2
Pd/CZa	372	265	386	315	423	305	443	383
Pd/CZLa	283	238	279	240	331	263	346	294
Pd/CZNa	307	259	316	262	345	271	348	311
Pd/CZPa	339	253	353	279	367	268	395	348
Pd/CZSa	385	278	403	297	472	351	–	386
Pd/CZYa	412	288	466	309	467	367	–	448

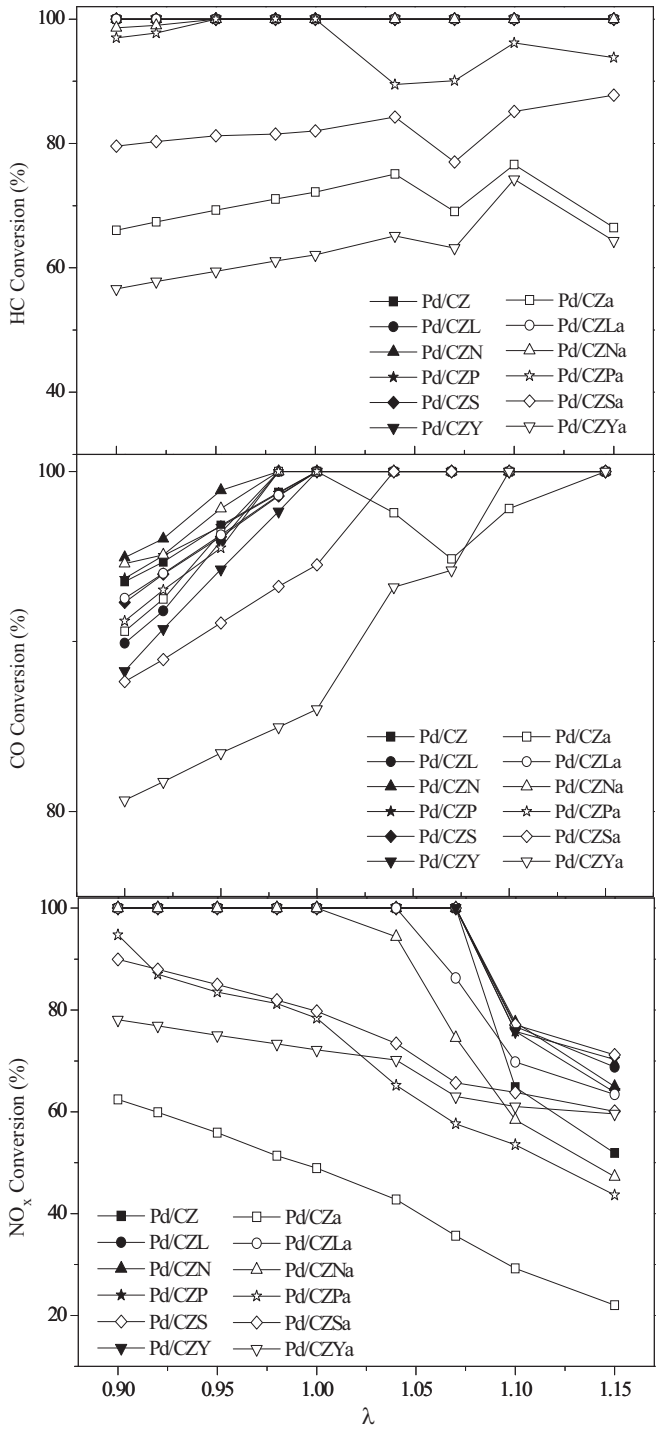

Fig. 9. Conversion curves of HC, CO and NO_x as a function of air/fuel ratio (λ) over the fresh and aged catalysts.

moting the catalytic performance of all the target pollutants. On the contrary, Pd/CZSa and Pd/CZYa show lower catalytic activity than Pd/CZa. What is more serious is that NO even cannot be transformed completely over Pd/CZSa and Pd/CZYa in the whole testing range. It is worthwhile to note that the catalytic activity of HC, CO, NO and NO_2 over the aged catalysts follows the same order: Pd/CZLa > Pd/CZNa > Pd/CZPa > Pd/CZa > Pd/CZSa > Pd/CZYa. From Fig. 7B, it can be seen that the temperature of peak α increases in the sequence of Pd/CZLa < Pd/CZNa < Pd/CZPa < Pd/CZa < Pd/CZSa < Pd/CZYa. This observation means that the catalytic activity of TWC could be related to the reducibility of PdO, and the higher the reducibility of the PdO species (namely, the lower the reduction temperature of PdO), the better the catalytic activity. Moreover, the existence of large amount of stable PdO in the case of Pd/CZLa, Pd/CZNa and Pd/CZPa (as mentioned in Section 3.4) is also accountable for their relatively higher catalytic performance.

Fig. 9 displays the results of air/fuel (λ) test over all the fresh and aged catalysts. As shown in Fig. 9, for all the fresh catalysts, the conversion of HC achieves 100% and the conversion of CO is higher than 80% in the whole air/fuel testing range, indicating the efficient catalytic activity of the fresh catalysts under oscillating feed gas composition. For the catalytic conversion of NO_x, all the fresh catalysts show 100% conversion under the lean oxygen conditions. Moreover, the NO_x operation window is enlarged obviously due to the modification of rare earth. According to literature [25,56], the oxygen vacancies associated with the Ce^{3+} ions near the noble metal particles in CZ-supported catalysts are the active sites for NO_x activation. Therefore, we can conclude that the higher DOSC caused by rare earth doping is one of the main reasons for the wide operation window of NO_x. For the aged catalysts, the operation window of Pd/CZa is destroyed obviously due to the pronounced decline of the dynamic oxygen storage capacity. From Fig. 9, it can be seen that the conversion of HC and NO_x is lower than 80% in the whole air/fuel testing range. However, the operation window is enlarged obviously due to the appearance of La, Nd and Pr. It has been shown in Fig. 5 that the DOSC of Pd/CZLa, Pd/CZNa and Pd/CZPa are higher than that of Pd/CZa. This observation indicates that the higher DOSC is related to the wider air/fuel operation window again. What should be mentioned is that the conversion of HC also reaches 100% over Pd/CZLa in the whole air/fuel measuring range. Moreover, Pd/CZLa also shows the widest operation window for NO_x among all the aged catalysts due to the highest DOSC before or after aged.

4. Conclusion

In this study, the influence of rare earth doping on the physicochemical properties of model $Ce_{0.2}Zr_{0.8}O_2$ solid solution and the three-way catalytic performance of its supported Pd-only catalyst has been investigated, and the following conclusions can be summarized:

(1) The formation of ceria–zirconia-rare earth ternary solid solution is confirmed by the results of XRD, and Zr is substituted by

rare earth element mainly in the crystal lattice. All the supports feature tetragonal structure due to Zr-rich in the component, no matter fresh and aged. The addition of rare earth would attenuate the sintering of solid solution, leading to the improved thermal stability.

(2) All the rare earth doped supports show higher BET surface area than CZ. CZLa, CZNa and CZPa also exhibit relatively bigger BET surface area even after calcination at 1100 °C for 4 h. The addition of La, Nd, Pr, Sm and Y is beneficial to enhance the relative concentration of Ce^{3+} on the surface of catalysts, which is the main reason for the increased DOSC.

(3) The ceria–zirconia solid solution doped with La, Nd and Pr and the corresponding catalysts exhibit improved reducibility and increased strong metal–support interaction, especially for the aged ones, which can inhibit the sintering of active PdO species. Therefore, Pd/CZLa, Pd/CZNa and Pd/CZPa present relatively higher three-way catalytic activity for all the target pollutants. The air/fuel operation window is also enlarged due to the increased DOSC.

Acknowledgements

The authors would like to acknowledge the Ministry of Science and Technology of China for the financial support of Project 2009AA064804 and the Science and Technology Department of Zhejiang Province for the financial support of Project 2009R50020. Moreover, we would also grateful to Professor Meiqing Shen at Key Laboratory for Green Chemical Technology of State Education Ministry, School of Chemical Engineering & Technology, Tianjin University for the dynamic oxygen storage capacity experiment.

References

[1] L.N. Ikryannikova, A.A. Aksenov, G.L. Markaryan, G.P. Murav'eva, B.G. Kostyuk, A.N. Kharlanov, E.V. Lunina, Appl. Catal. A: Gen. 210 (2001) 225–235.
[2] H. Birgersson, L. Eriksson, M. Boutonnet, S.G. Järås, Appl. Catal. B: Environ. 54 (2004) 193–200.
[3] A. Morikawa, T. Suzuki, T. Kanazawa, K. Kikuta, A. Suda, H. Shinjo, Appl. Catal. B: Environ. 78 (2008) 210–221.
[4] H. Vidal, J. Kašpar, M. Pijolat, G. Colon, S. Bernal, A. Cordón, V. Perrichon, F. Fally, Appl. Catal. B: Environ. 30 (2001) 75–85.
[5] P.S. Lambrou, C.N. Costa, S.Y. Christou, A.M. Efstathiou, Appl. Catal. B: Environ. 54 (2004) 237–250.
[6] M. Zhao, M. Shen, J. Wang, J. Catal. 248 (2007) 258–267.
[7] J. Kašpar, P. Fornasiero, N. Hickey, Catal. Today 77 (2003) 419–449.
[8] S. Matsumoto, Catal. Today 90 (2004) 183–190.
[9] A.I. Kozlov, D.H. Kim, A. Yezerets, P. Anderson, H.H. Kung, M.C. Kung, J. Catal. 209 (2002) 417–426.
[10] M. Ozawa, J. Alloys Compd. 272–277 (1998) 886–890.
[11] P. Fornasiero, J. Kašpar, V. Sergo, M. Graziani, J. Catal. 182 (1999) 56–59.
[12] G. Balducci, J. Kašpar, P. Fornasiero, M. Graziani, M. Saiful Islam, J.D. Gale, J. Phys. Chem. B 101 (1997) 1750–1753.
[13] G. Balducci, J. Kašpar, P. Fornasiero, M. Graziani, M. Saiful Islam, J. Phys. Chem. B 102 (1998) 557–561.
[14] H.C. Yao, Y.F. Yu Yao, J. Catal. 86 (1984) 254–265.
[15] J. Kašpar, R. Di Monte, P. Fornasiero, M. Graziani, H. Bradshaw, C. Norman, Top. Catal. 16 (2001) 83–87.
[16] S. Bedrane, C. Descorme, D. Duprez, Catal. Today 73 (2002) 233–238.
[17] P. Fonasiero, R. Di Monte, G. Ranga Rao, J. Kašpar, S. Meriani, A. Trovarelli, M. Graziani, J. Catal. 151 (1995) 168–177.
[18] S. Suhonen, M. Valden, M. Hietikko, R. Laitinen, A. Savimäki, M. Härkönen, Appl. Catal. A: Gen. 218 (2001) 151–160.
[19] J.R. González-Velasco, M.A. Gutiérrez-Ortiz, J.L. Marc, J.A. Botas, M.P. González-Marcos, G. Blanchard, Appl. Catal. B: Environ. 25 (2000) 19–29.
[20] H. Vidal, J. Kašpar, M. Pijolat, G. Colon, S. Bernal, A. Cordón, V. Perrichon, F. Fally, Appl. Catal. B: Environ. 27 (2000) 49–63.
[21] S. Larrondo, M.A. Vidal, B. Irigoyen, A.F. Craievich, D.G. Lamas, I.O. Fábregas, G.E. Lascalea, N.E. Walsöe de Reca, N. Amadeo, Catal. Today 107–108 (2005) 53–59.
[22] Y. Guo, G. Lu, Z. Zhang, S. Zhang, Y. Qi, Y. Liu, Catal. Today 126 (2007) 296–302.
[23] M.H. Youn, J.G. Seo, K.M. Cho, S. Park, D.R. Park, J.C. Jung, I.K. Song, Int. J. Hydrogen Energy 33 (2008) 5052–5059.
[24] H. Wang, Y. Chen, Q. Zhang, Q. Zhu, M. Gong, M. Zhao, J. Nat. Gas Chem. 18 (2009) 211–216.
[25] P. Vidmar, P. Fornasiero, J. Kašpar, M. Graziani, J. Catal. 171 (1997) 160–168.
[26] M. Boaro, C. Leitenburg, G. Dolcetti, A. Trovarelli, J. Catal. 193 (2000) 338–347.
[27] P. Fornasiero, N. Hickey, J. Kašpar, C. Dossi, D. Gava, M. Graziani, J. Catal. 189 (2000) 326–338.
[28] H. He, H.X. Dai, L.H. Ng, K.W. Wong, C.T. Au, J. Catal. 206 (2002) 1–13.
[29] E.V. Frolova, M. Ivanovskaya, V. Sadykov, G. Alikina, A. Lukashevich, S. Neophytides, Prog. Solid State Chem. 33 (2005) 317–325.
[30] X. Wu, X. Wu, Q. Liang, J. Fan, D. Weng, Z. Xie, S. Wei, Solid State Sci. 9 (2007) 636–643.
[31] J. Fan, X. Wu, L. Yang, D. Weng, Catal. Today 126 (2007) 303–312.
[32] F. Dong, T. Tanave, A. Suda, N. Takahashi, H. Sovukawa, H. Shinjoh, Chem. Eng. Sci. 63 (2008) 5020–5027.
[33] Q. Wang, B. Zhao, G. Li, R. Zhou, Environ. Sci. Technol. 44 (2010) 3870–3875.
[34] A. Papavasiliou, A. Tsetsekou, V. Matsouka, M. Konsolakis, I.V. Yentekakis, N. Boukos, Appl. Catal. B: Environ. 90 (2009) 162–174.
[35] Q. Wang, G. Li, B. Zhao, R. Zhou, Appl. Catal. B: Environ. 100 (2010) 516–528.
[36] L. Martín, J.L. Arranz, O. Prieto, R. Trujillano, M.J. Holgado, M.A. Galán, V. Rives, Appl. Catal. B: Environ. 44 (2003) 41–52.
[37] J. Fan, X. Wu, X. Wu, Q. Liang, R. Ran, D. Weng, Appl. Catal. B: Environ. 81 (2008) 38–48.
[38] F.B. Noronha, E.C. Fendley, R.R. Soares, W.E. Alvarez, D.E. Resasco, Chem. Eng. J. 82 (2001) 21–31.
[39] J. Fan, D. Weng, X. Wu, X. Wu, R. Ran, J. Catal. 258 (2008) 177–186.
[40] C. Bozo, N. Guilhaume, J.-M. Herrmann, J. Catal. 203 (2001) 393–406.
[41] Q. Wang, G. Li, B. Zhao, M. Shen, R. Zhou, Appl. Catal. B: Environ. 101 (2010) 150–159.
[42] N. Hickey, P. Fornasiero, J. Kašpar, J.M. Gatica, S. Bernal, J. Catal. 200 (2001) 181–193.
[43] C. Descorme, R. Taha, N. Mouaddib-Moral, D. Duprez, Appl. Catal. A: Gen. 223 (2002) 287–299.
[44] M. Boaro, F. Giordano, S. Recchia, V.D. Santo, M. Giona, A. Trovarelli, Appl. Catal. B: Environ. 52 (2004) 225–237.
[45] S. Hilaire, X. Wang, T. Luo, R.J. Gorte, J. Wagner, Appl. Catal. A: Gen. 215 (2001) 271–278.
[46] S.Y. Christou, C.N. Costa, A.M. Efstathiou, Top. Catal. 30/31 (2004) 325–331.
[47] C.N. Costa, S.Y. Christou, G. Georgiou, A.M. Efstathiou, J. Catal. 219 (2003) 259–272.
[48] S. Salasc, V. Perrichon, M. Perrichon, M. Primet, N. Mouaddib-Moral, J. Catal. 206 (2002) 82–90.
[49] W. Lin, Y.X. Zhu, N.Z. Wu, Y.C. Xie, I. Murwani, E. Kemnitz, Appl. Catal. B: Environ. 50 (2004) 59–66.
[50] M.P. Yeste, J.C. Hernández, S. Bernal, G. Blanco, J.J. Calvino, J.A. Pérez-Omil, J.M. Pintado, Catal. Today 141 (2009) 409–414.
[51] J. Kašpar, P. Fornasiero, M. Graziani, Catal. Today 50 (1999) 285–298.
[52] J. Wang, M. Shen, Y. An, J. Wang, Catal. Commun. 10 (2008) 103–107.
[53] I. Atribak, A. Bueno-López, A. García-García, J. Catal. 259 (2008) 123–132.
[54] P.S. Lambrou, A.M. Efstathiou, J. Catal. 240 (2006) 182–193.
[55] G. Li, B. Zhao, Q. Wang, R. Zhou, Appl. Catal. B: Environ. 97 (2010) 41–48.
[56] G. Ranga Rao, P. Fornasiero, R. Di Monte, J. Kašpar, G. Vlaic, G. Balducci, S. Meriani, G. Gubitosa, A. Cremona, M. Graziani, J. Catal. 162 (1996) 1–9.